**Title :**

Harvesting Far-red Light by Chlorophyll *f* in Photosystems I and II of Unicellular Cyanobacterium strain KC1.

**Running title :** Chlorophyll *f* in PS I and II of cyanobacterium strain KC1

**Corresponding Author:**

Shigeru Itoh
Center for Gene Research, Nagoya University, Furocho, Chikusa, Nagoya 464-8602, Japan
tel/fax; +81-52-789-2401
e-mail; itoh2nd@gmail.com

**Subject area**: 3) photosynthesis, respiration and bioenergetics

**Number of black and white figures**, 0. **colored figures**, 6

**Number of supplementary materials**, 5 figures

**Title :**

Harvesting Far-red Light by Chlorophyll *f* in Photosystems I and II of Unicellular Cyanobacterium strain KC1

**Running head :** Chlorophyll *f* in PS I and II of cyanobacterium strain KC1

**Authors :**

Shigeru Itoh[1], Tomoki Ohno,[2] Tomoyasu Noji,[3] Hisanori Yamakawa,[4] Hirohisa Komatsu,[5] Katsuhiro Wada,[5] Masami Kobayashi[5] and Hideaki Miyashita[2, 6]

[1]Center for Gene Research, Nagoya University, Furo-cho, Chikusa, Nagoya 464-8602, Japan
[2]Graduate School of Human and Environmental Studies, Kyoto University, Kyoto 606-8501, Japan
[3]Department of Frontier Materials, Graduate School of Engineering, Nagoya Institute of Technology, Gokiso-cho, Showa, Nagoya 466-8555, Japan
[4]Graduate School of Bioagricultural Sciences, Nagoya University, Furo-cho, Chikusa, Nagoya 464-8602, Japan
[5]Division of Materials Science, Faculty of Pure and Applied Science, University of Tsukuba, Tsukuba, Ibaraki 305-8573, Japan
[6]Graduate School of Global and Environmental Studies, Kyoto University, Kyoto 606-8501, Japan

**Abbreviations**: APC, allophycocyanin; Chl, chlorophyll; DAS, decay-associated spectrum; Fr and Wh cells, cells grown under far-red and white light, respectively; PC, phycocyanin; PE, phycoerythrin; Phe, pheophytin ; PSI and PSII, photosystems I and II; TRS, time-resolved spectrum

**Abstract:**

Cells of a unicellular cyanobacterium strain KC1, which was collected at Japanese freshwater Lake Biwa, formed chlorophyll (Chl) *f* at 6.7 % with respect to Chl *a* after the growth under 740 nm light. The far-red-acclimated cells (Fr cells) formed extra absorption bands of Chl *f* at 715 nm in addition to the Chl *a* bands present in the white-light-adapted cells (Wh cells). Fluorescence lifetimes of Chls were measured. The 405-nm laser flash, which excites mainly Chl *a* in photosystem I (PS I), induced a fast energy transfer to multiple fluorescence bands at 720–760 and 805 nm of Chl *f* at 77 K in Fr cells with almost no PSI red-Chl *a* band. The 630-nm laser flash, which mainly excited PSII through phycocyanin (PC), revealed fast energy transfer to another set of Chl *f* bands at 720-770 and 810 nm as well as to the 694-nm Chl *a* fluorescence band. The 694-nm band no more transferred excitation energy to Chl *f*. Therefore, Chl *a* in PSI, and phycocyanin in PSII of Fr cells transferred excitation energy to different sets of Chl *f* molecules. Multiple Chl *f* forms, thus, seem to work as the far-red antenna both in PSI and PSII. A variety of cyanobacterial species, phylogenically distant from each other, are shown to use Chl *f*-antenna under the far-red environments, such as under dense biomats, colonies, or under far-red LED light.

**Key words:** chlorophyll *f*, cyanobacteria, far-red light, light harvesting, PSI, PSII

***Introduction***

Oxygen-evolving photosynthesis of plants and cyanobacteria uses chlorophyll *a* (Chl *a*) as a major pigment except for some cases. Chl *a* harvests visible light and undergoes charge separation in photosystems I and II (PSI and PSII) reaction center complexes as revealed by the structural analyses (Jordan et al. 2001, Umena et al. 2111). Only two other chlorophylls, divinyl-Chl *a* and Chl *d*, have been known to replace the function of Chl *a*. Divinyl-Chl *a* shows an absorption spectrum with a Qy band almost similar to that of Chl *a* and functions as a major pigment in cyanobacteria belonging to *Prochlorophyta* (see a review by Lewin, 2002). On the other hand, Chl *d*, which absorbs far-red light at 700–740 nm (Miyashita et al. 1996, 1997, Schliep et al. 2010, Miller et al. 2005, Murakami et al. 2004), is also used both as the special pair and a major light-harvesting pigment in PSI (Hu et al. 1998) and PSII (Itoh et al. 2001, 2007, Tomo et al. 2007) in *Acaryochloris* species. *Acaryochloris* cells have a small amount (5%) of Chl *a* too, in which one or two molecules work as the primary electron acceptor $A_0$ in PSI (Kumazaki et al. 2002). Chl *d* is a derivative of Chl *a* with a formyl group attached to C3 atom on ring I of the chlorin macrocycle (see Fig. S1).

A filamentous cyanobacterium, *Halomicronema hongdechloris*, collected on the Australian coast, was recently shown to produce another far-red-absorbing chlorophyll species, Chl *f* (Chen et al. 2010, 2012, and see Figs. S1). Chl *f*, which is formed only after growth under far-red light, absorbs light mainly at 720 nm, at a wavelength a little longer than Chl *d*, and gives a fluorescence peak at 740 nm *in vivo* (Li et al. 2012, Chen et al. 2010, 2012, 2014, see Fig. S2). Recent studies have reported Chl *f* productions also in a unicellular fresh water cyanobacterium strain KC1 (Akutsu et al. 2011, Ohkubo et al. 2011, Miyashita et al. 2014) and a filamentous thermophilic cyanobacterium, *Leptolyngbya* sp. strain JSC-1 (Gan et al. 2014). The latter work suggested that the far-red-absorbing sensory GAF domain proteins trigger biosynthesis of Chl *f*, and expression of new antenna and reaction center proteins. Chl *f* is a derivative of Chl *a* with additional formyl group on C2, (but not on C3 as in the case of Chl *d*) in ring I of the chlorin macrocycle (See Figs. S1 and S2 for the chemical formula and optical properties). However, Chl *f* has been identified as a “minor” component that was formed only under far-red light (Chen et al. 2010, 2012, Gan et al. 2014, Akutsu et al. 2011) in addition to the major pigment Chl *a*. The situation is, therefore, somewhat different from that of divinyl Chl *a* or Chl *d*, which are produced constitutively as the major pigments even under white light (Miyashita et al. 1996, 1997, Miller et al. 2005, Murakami et al. 2004, Hu et al. 1998, Itoh et al. 2001, 2007, Tomo et al. 2007). The function of Chl *f* has not been clear yet.

The biosynthesis pathway of Chl *d* has not yet been clear even after extensive genomic analysis (Schliep et al. 2010, Gan et al. 2014, Mielke et al. 2011, Swingley et al. 2008) although its function as the antenna and reaction center pigments has been almost established (Hu et al. 1998,

Itoh et al. 2001, 2007, Tomo et al. 2007). The biosynthesis pathway and function of Chl *f* have neither been clear yet (Gan et al. 2014) although the physicochemical properties of isolated Chl *f* have been characterized (Li et al. 2013, Niedzwiedzki et al. 2014, Willows et al. 2013). Absorption and fluorescence spectra of Chl *f* show Qy bands at the wavelengths longer than those of Chls *a* and *d* (see Fig. S2). The locations and functions of Chl *f* molecules in PSI or PSII have not been known yet. Recent works (Tomo et al. 2014, Akimoto et al. 2015) analyzed fluorescence lifetimes of pigments excited by the 440-nm laser flash in cells and isolated thylakoids of *H. hongdechloris*, and concluded that Chl *f* accepts excitation energy rapidly from Chl *a* with the fast 0.5 and 1.2 ps time constants.

In this paper we studied the function of Chl *f* in a unicellular cyanobacterium strain KC1 that was isolated from Japanese inland freshwater Lake Biwa (Akutsu et al. 2011, Ohkubo et al. 2011, Miyashita et al. 2014). KC1 cells formed Chl *f* at 6.7 % with respect to Chl *a* (see Table 1), as a minor component after growth under far-red light (Akutsu et al. 2011, Miyashita et al. 2014) like the other two species (Chen et al. 2010, Gan et al. 2014). On the other hand, phylogenic location of KC1 strain is very distant from *H. hongdechloris* and *Leptolyngbya* sp. and is rather closer to *Acaryochloris* (Miyashita et al. 2014). Therefore, it is not clear whether Chl *f* functions similarly in the distant Chl *f*-producing species or not. In this study the function of Chl *f* in the KC1 cells, which were grown for 3 weeks under 740 nm LED light (designated as Fr cells hereafter), was studied by analyzing the energy transfer process at 300 and 77 K. It will be shown that Chl *f* molecules accept excitation energy from Chl *a* in PSI rapidly in Fr cells as reported in *H. hongdechloris* (Tomo et al. 2014, Akimoto et al. 2015), and that phycocyanin transfers excitation energy to another set of Chl *f* molecules in PSII. It is also found that Chl *f* gives unique long-wavelength emission bands at 805 and 810 nm, respectively, in PSI and PSII at 77 K. The two different sets of Chl *f* molecules, thus, seem to function as the far-red antenna in PSI and PSII of KC1 cells.

***Results***

*Absorption bands of Chl f in KC1 cells*. KC1 cells show round unicellular shapes with diameters of a few μ□ as shown by an inset microscopic image in Fig. 1 as reported (Miyashita et al. 2014). The cell shapes are very different from those of filamentous cells of a marine cyanobacterium *H. hongdechloris* that was found to produce Chl *f* first (Chen et al. 2010) or of thermophilic *Leptolyngbya* sp. (Gan et al. 2014). KC1 cells grown under white light and 740 nm LED light for three weeks are designated as Wh and Fr cells, respectively, hereafter. As shown in Fig. 1, Wh cells show absorption peaks of Chl *a* at 437 and 678 nm, carotenoids at 450–530 nm, phycoerythrin (PE) at 570 nm and phycocyanin (PC) at 625 nm and allophycocyanin (APC) presumably at around 650 nm, as typical for cyanobacteria (Murakami et al. 1997, Hirose et al. 2013). Fr cells showed a lower

PE band and higher PC/APC band with respect to the Chl *a* band, and a new wide peak at 715 nm of Chl *f* as reported (Akutsu et al. 2011, Miyashita et al. 2014). The new band can be assigned to be Chl *f* in comparison with the absorption spectrum of purified Chl *f* in benzene that gives an absorption peak at 701 nm (see Fig. S2). The loss of PE and the increase of PC/APC seem to reflect the "chromatic acclimation", in which PE formation is triggered by green light and suppressed by red light (Murakami et al. 1997, Hirose et al. 2013). The 740 nm light thus not only suppresses the PE synthesis but also induces biosynthesis of Chl *f*. The absorption spectra of Fr cells resemble those reported for cells of *H. hongdechloris* (14) or *Leptolyngbya* sp. (Gan et al. 2014) grown under far-red light.

Pigment contents of cells were determined by HPLC after extraction with acetone/methanol (7/3, v/v) mixture as described in Materials and Methods (Table 1). Wh and Fr cells contained 0 and 6.7 % Chl *f*, respectively, with respect to Chl *a*. The amount of Chl *f* at 6.7 % is higher than that of Chl *a'* at 2.0 %, which is expected to comprise (a half of) a special pair P700 in PSI, or of pheophytin (Pheo) *a* at 1 %, two of which are expected to work as the electron acceptor in PSII. Therefore, it seems that several Chl *f* molecules are present either in PSI or PSII, or in both photosystems. Although the Chl *a*' contents were similar between Wh and Fr cells, Pheo *a* content in Fr cell was 2/3 that in Wh cell suggesting a partial decrease of PSII content after far-red acclimation.

*Steady state fluorescence spectra of Wh and Fr cells at room temperature and at 77 K.* Fluorescence spectra of Wh and Fr cells were measured (Fig. 2). The fluorescence spectrum of Wh cells excited by 570 nm light, which excites PE preferentially, showed peaks of PE (below 600 nm), PC/APC (at around 658 nm) and PSII Chl *a* (684 nm) and a shoulder at 715 nm of PSI Chl *a* (red line in Fig. 2a). The peak wavelengths of bands were estimated based on the 2$^{nd}$ derivative spectra calculated from the emission spectra. The three shorter-wavelength bands of PE, PC/APC and Chl *a* (684 nm) can be assigned to be associated with PSII, and the 715-nm shoulder mainly with "red-Chl *a*", which has been assumed to be aggregated forms of Chl *a* on PSI (Gobets et al. 2001, Komura and Itoh 2009). On the other hand, the excitation by 440 nm light, which mainly excites antenna Chl *a* on PSI, induced a distinct 715 nm band of PSI red-Chl *a* showing the fast energy accumulation to red-Chl *a*, together with a 684-nm PSII band. The 570-nm and 440-nm excitation light, therefore, almost specifically excited PSII and PSI, respectively, as well known in cyanobacterial cells (Gobets et al. 2001, Murakami et al. 1997, Sugiura and Itoh 2012).

Figure 2b shows fluorescence spectra measured in Fr cells. The 570 nm excitation light induced fluorescence bands at 658 nm of PC/APC and at 684 nm of PSII-Chl *a* together with a large band at 722 nm (blue line). The 440 nm excitation light, on the other hand, induced a large 727 nm band instead of the 715-nm red-Chl *a* band, with a smaller PSII Chl *a* band at 683 nm (red

line). The shift of the peak wavelength of the red-most 727-nm peak in the 440-nm excited spectrum by 5 nm from the 722-nm peak in the 570-nm excited spectrum might represent their different origin as discussed below based on the 77 K spectra.

Fluorescence spectra were also measured at 77 K. At low temperature overlapping bands are better resolved due to the narrowing of bandwidths, and the longer wavelength bands are more enhanced by the excitation energy accumulation from the shorter-wavelengths, higher-energy-level bands. The spectrum excited by 440 nm light in Wh cells (Fig. 2c, red line) revealed small fluorescence bands at around 687/694 nm (PSII Chl *a*) together with a large 731 nm band with a 40 nm wide bandwidth emitted from PSI red-Chl *a*. The excitation at 570 nm (blue line) induced fluorescence bands of PE (shorter than 600 nm), PC/APC at 646/662 nm, and PSII Chl *a* at 687 nm that are stronger than the red-Chl *a* band.

The spectrum at 77 K in Fr cells excited by 440 nm light (Fig. 2d, red line) showed small emission bands at 662 nm (PC/APC) and 693 nm (PSII Chl *a*). A large, narrow, 748 nm band was detected too. However, the broad 731-nm red-Chl *a* band, which was present in the Wh-cells in Fig. 2c, was not detected. The spectrum is almost the same as that reported in the far-red-acclimated *H. hongdechloris* cells measured with the excitation at 405 nm at 77 K (Chen et al. 2012) or in *Leptolyngbya* sp. cells (Gan et al. 2014). The 748 nm peak with a narrow 20 nm bandwidth seems to be assigned to a Chl *f* emission band as assigned before (Chen et al. 2012, Gan et al. 2014, Miyashita et al. 2014). As shown in the excitation spectra at 77 K in Fig. S3 D, this band was specifically excited by the light at 440 and 670 nm that mainly excites Chl *a* in PSI.

The fluorescence spectrum of Fr cells excited at 570 nm (Fig. 2d, blue line) showed a very different emission spectrum. It showed high PC/APC peaks at 646/662 nm, a Chl *a* peak at 693 nm, together with the peak at about 750 nm with more pronounced shoulder bands at 720, 736 and 760 nm. The relative contribution of 750 nm narrow band was smaller compared to that in the 440 nm-excited spectrum. The bands at around 800 nm, which should be present (see Figs. 4 and 5 and later sections), could not be identified well in this measurement with the low sensitivity around 800 nm. The feature at 735–780 nm was different from those in Fig. 2c. It is, therefore, clear that the pigments absorbing at 550–650 nm on phycobilisome (mainly PC) transfer excitation energy to the 720-760 nm Chl *f* bands. Excitation spectra for the 745-nm and 730-nm emission bands were different each other (Fig S3, D). The high Chl *f* fluorescence bands, however, do not seem to be induced by the direct excitation of Chl *f* absorption bands itself because of the low content of Chl *f* at 6.7 % (Table 1) and the expected smaller absorption of Chl *f* compared to Chl *a* in Fig. 1. The excitation spectra shown in Fig. S3, together with absorption and emission spectra of purified Chl *f* in benzene (Fig. S2), indicate the energy transfer to Chl *f* from other pigments.

Fluorescence spectra in Fig. 2 (and Fig. S3), which resemble those reported in other

species (Chen et al. 2010, Gan et al. 2014), however, were measured with a conventional fluorescence spectrometer that has low sensitivities above 750 nm, and the spectra were presented without correction of the detector sensitivity that falls sharply above 700 nm. In the next section, sensitivity-corrected emission spectra, as well as the lifetimes, were studied by the measurements with the streak camera system that uses a CCD detector with significantly better sensitivities and time resolution as described elsewhere (Komura and Itoh, 2009).

*Fluorescence lifetime analysis at room temperature.* Fluorescence emission spectra and lifetimes were measured simultaneously at room temperature in Fr cells, and were presented as wavelength-time two-dimensional images (Fig. 3 a and b). Fluorescence was excited by diode laser flash of 50 ps duration, either at 405 nm or 630 nm, and was detected with a streak camera in the photon-counting mode, and the images and spectra were displayed after correction for sensor sensitivities in every case.

Fig. 3a shows two-dimensional image (horizontal axis represents wavelength and vertical axis, time delay with respect to the peak time of excitation laser pulse) of sensitivity-corrected fluorescence emission obtained in Fr cells after 405 nm excitation laser pulse at room temperature. Fluorescence showed the brightest spot at 760 nm at 0.1 ns (Fig. 3a) after the excitation by the 405-nm laser flash, which was detected separately and not shown. The horizontal envelope of bright area extended to 850 nm, showing a wide emission bandwidth. The intensity rapidly decreased within 1 ns, as seen from the short vertical tail.

Fluorescence excited by the 630-nm laser (Fig. 3b) showed a little wider spectrum extending to 850 nm, giving the brightest spot at 760 nm. A weaker fluorescence band at around 680 nm of PSII Chl *a* is also seen in the image. The image is, therefore, a little different from that in Wh cells, which showed the large broad red-Chl *a* band at 745 nm and lacked Chl *f* bands (not shown, see time resolved spectra of Wh cell in Fig. S4).

*Fluorescence lifetime analysis at 77 K.* Fluorescence decay was also measured at 77 K in Fr cells. Excitation at 405 nm induced the brightest spot at 740-50 nm first (Fig. 3c). The bright area became narrower in a very short time, and then, lasted long time at 748 nm. A separate spot at 805 nm was also detected clearly in this sensitivity-corrected image. The 805-nm spot showed the lifetime shorter than that at 748 nm.

The excitation by 630-nm laser, on the other hand, induced a different image with a larger number of spots (Fig. 3d). Bright spots are observed first at 665 (PC), 695 (PSII Chl *a*), 720–760, and 810 nm. The bands at 665 and 695 nm, which were scarce in the 405 nm-excited image, can be assigned to the emission from PC/APC and PSII Chl *a*-695, respectively. The bands at 720–820 nm can be assigned to Chl *f* emission. The images induced by the 405 and 630 nm laser excitations are

very different each other.

*Sensitivity-corrected fluorescence emission spectra with large bands at 805-810 nm.* All the photons detected at 0-5 ns in Figs. 3c were integrated to calculate the integrated fluorescence spectrum in Fig. 3e, which is equivalent to the emission spectrum under continuous excitation. The integrated 405 nm-excited spectrum at 77 K in Fig. 3e, which is corrected as for detector sensitivity too, showed a major peak at 748 nm with a shoulder band at 805 nm. On the other hand, the corrected 630 nm-excited spectrum in Fig. 3f, calculated from Fig. 3d, showed peaks at 690, 750 and 810 nm. Both spectra showed high peaks at around 750 nm, and exhibited other bands at 805-810 nm, which could not be resolved well in the sensitivity-uncorrected spectra such as those in Fig. 2 or in previous reports (Chen et al. 2010, Gan et al. 2014, Miyashita et al. 2014, Tomo et al. 2014, Sugimoto et al. 2015). When both spectra are displayed to overlap each other (Fig 3e, thick and thin lines), it is clear that they are a little different from each other, suggesting the emission from different sets of Chl *f*. Therefore, PSI and PSII appear to contain different sets of Chl *f* molecules.

*Time-resolved spectrum (TRS).* The fluorescence images measured at 77 K in Fig. 3c and d were further analyzed by calculating time-resolved spectra (TRS) to see the variation of spectra after the laser excitation (Fig. 4). Each TRS was calculated from Fig. 3c image for a central delay time at -0.12 - 4.2 ns after the laser excitation. TRS curves calculated from the 405 nm-excited image in Fig 3c showed peaks at around 695, 735, 747, 760 and 806 nm (Fig. 4a). The bandwidth of the central highest band at around 750 nm became narrower with time and finally gave a sharp 20 nm bandwidth peaking at 748 nm. We designate this 748 nm band that has the longest lifetime as F748. The intensities at 735, 760 and 805 nm decayed faster compared to the 748-nm peak intensity.

A TRS at 0.12 ns calculated from the 630 nm-excited image in Fig. 3d showed multiple peaks at 665, 695, 730, 752, 760 and 810 nm (Fig. 4b). Narrowing of bandwidth at 730–760 nm to 752 nm at 0- 1.7 ns indicates the faster decaying components at around 730 and 760 nm. The peak at 695 nm of PSII-Chl *a* was strong and was detected until 4.2 ns. The peak at 752 nm, whose position is a little longer than that of F748, also remained till 4.2 ns. Therefore, 405- and 630-nm excitations induced fluorescence from different sets of Chl *f* spectral forms.

TRS of the Wh-cell excited by the 405-nm laser at room temperature and at 77K was also calculated (Fig. S4). TRS analysis at 300 K showed emission peaks at around 685 nm (PSII Chl *a*) and a large, wide band of PSI red-Chl *a* at 725 nm (Fig. S4 a). The analysis at 77 K (Fig. S4 b) showed a large, wide band of PSI red-Chl *a* at 740 nm, which wavelength is red-shifted by the sensitivity correction from 732 nm in the uncorrected spectra in Fig. 2. Analysis of lifetime indicated this band to decay with a major and minor lifetime components of 0.4 ns (90%) and 1.1 ns (10 %) (not shown). No peaks were detected at 805-810 nm in this case indicating no contribution

from Chl *f*. The TRS of Wh-cell, therefore, is significantly different from that in Fr cell. It also indicates almost no contribution of the red-Chl *a* to the TRS of Fr cells in Fig. 4.

TRS in Fr cells at room temperature was calculated from Figs. 3 c and d and shown in Fig. S5. The 405-nm laser induced the 680-nm Chl *a* peak and broad bands at 750 and 800 nm (Fig. S5 a). The spectral shape did not significantly change at 0.22-1.4 ns. TRS calculated from the 630-nm-excited image at room temperature showed peaks at 660-680, 730- and 810-nm (Fig.S6 b). The peaks at 660-680 nm, as well as that at 730 nm are more marked indicating the higher contribution of the shorter wavelength peaks compared to those in the 405-nm-excited TRS. Also in this case, the spectral shape did not change significantly at 0.22-1.4 ns suggesting the fast equilibration of excitation energy at room temperature. The energy transfer process will be discussed in more detail in the next section.

*Analysis of energy transfer based on decay-associated spectrum (DAS) at room temperature.* Energy transfer was further analyzed in Fr cells by calculating the decay-associated spectra (DAS) by global analysis of the images in Fig. 3 as described in ***Materials and Methods***. Each DAS curve is formed by rise or/and decay of fluorescence bands that are changing with a same time constant ($t_c$) (Fig. 5). Positive and negative bands in a same DAS curve represent energy transfers from components fluorescent in positive-amplitude regions to those in the negative-amplitude region

The 405 nm-excited fluorescence image in Fig. 3a at room temperature can be interpreted by four DAS curves. The DAS with the shortest $t_c$ (a black line, with a $t_c$ <0.02 ns) gave a positive band at 690 nm and a broad negative band above 730 nm. The curve suggests a fast energy transfer (<0.02 ns) from the Chl *a* band centered at 680-690 nm to the multiple Chl *f* forms that give fluorescence at 740–850 nm. DAS curves with the longer time constants showed only positive peaks at 760 (red, with a 0.13-ns $t_c$), 795 (blue, with a 0.20-ns $t_c$) and 750 nm (green, with a 0.80-ns $t_c$). These positive bands indicate the energy transfer/fluorescence emission from these Chl *f* bands after the fast energy transfer to them. Therefore, the excitation energy absorbed by Chl *a* at 405 nm gives emission at around 690 nm, and also is rapidly transferred to the multiple Chl *f* bands. The DAS with the longest $t_c$ of 0.8 ns gave a single peak at 750 nm.

DAS of the 630 nm-excited image (Fig. 5b) showed fast (a black line, with a $t_c$ <0.02-ns) decay (positive peaks) at 660 (phycocyanin) and 720 nm (probably Chl *f*) and suggested the rapid energy transfer to the Chl *f* bands at 740–820 nm, though the curve is rather noisy. Other DAS curves showed broad positive peaks at 730 and 790 nm (green, with a 0.22-ns $t_c$) and 750 nm (blue, with a 0.81-ns $t_c$) suggesting the fast (<0.02 ns) energy transfer from the PC/APC band to multiple Chl *f* bands at 730–820 nm. Energy transfer from the 720 nm band to the longer wavelength bands with a short $t_c$ at around 0.22 ns is suggested. On the other hand, the 750-nm band decayed slowly with a 0.81-ns $t_c$. The results indicate that excitation at 630 nm initiated the energy transfer process

that is different from that initiated by the 405 nm excitation.

*DAS analysis at 77 K*. Four DAS curves interpreted the image in Fig. 3c excited by the 405-nm laser at 77 K as shown in Fig. 5c. A DAS with the shortest $t_c$ of 0.05 ns showed positive peaks at 680-90, 720, 760 nm, and negative peaks at 750 and 805-10 nm (a black line). The 810-nm Chl *f* bands, therefore, accepts excitation energy from the photo-excited Chl *a* within 0.05 ns. It is also suggested that 720 and 760 nm Chl *f* bands are excited faster than 0.05 ns because the positive peaks at 720 and 760 nm represent only the decay of Chl *f* bands that have already accepted energy from PSI Chl *a*. Although such fast processes could not be resolved in the present experimental setup. It may correspond to the fast process such as the 0.005-ns energy transfer process from Chl *a* to Chl *f*, which is recently shown by Akimoto et al (2015) in *H. hongdechloris* cells. A DAS with a moderate $t_c$ of 0.19 ns (a red line) showed peaks at 740-760 and 805 nm. The DAS with a $t_c$ of 0.92 ns showed positive peaks at 690, 740 and 810 nm. The longest $t_c$ of 2.4 ns (a blue line) gave a single narrow peak at around 750 nm that corresponds to F748. Its long lifetime indicates that F748 does not transfer excitation energy to other bands at least at 77 K.

Four DAS curves interpreted the image (Fig. 3d) excited by the 630-nm laser at 77 K as shown in Fig. 5d. The fastest DAS with a 0.07-ns $t_c$ (a black line) showed positive peaks at 660 (APC) and 720 nm (Chl *f*) and negative ones at 740 and 810 nm. The 0.33-ns DAS (red) showed positive peaks at 680, 735, 760 and 810 nm. The 1.09-ns DAS (green) showed positive peaks at 680–690 and 740 nm, with a small peak at 770 nm. The 2.07-ns DAS (blue) showed a single positive peak at 750 nm. It is, therefore, assumed that the excitation energy is transferred from the PC/APC band at 660 nm to the Chl *f* band at 720 nm, and then to Chl *f* bands at 740 and 820 nm with a 0.07-ns $t_c$. The 720-nm Chl *f* band, thus, seems to accept excitation energy from PC within 0.07 ns, probably via Chl *a*. In the 0.33-ns DAS, a positive broad band at 680 nm seems to represent the emission (or energy transfer) from Chl *a* on PSII, while the positive bands at 730–740, 760 and 810 nm seem to represent the Chl *f* decay. A DAS with a 1.1-ns $t_c$ indicates the decays of 695-nm Chl *a* band of PSII and of 740- and 770-nm Chl *f* bands. The DAS that had the longest $t_c$ of 2.1 ns gave a narrow peak at 750 nm, which seems to be emitted from a Chl *f* species different from the one with a 2.4-ns $t_c$ in Fig. 5c excited by 405-nm laser, judging from the different peak positions. The longest lifetime components in PSI and PSII, thus, seem to be emitted from the different Chl *f* forms, both of which give narrow bands suggesting their monomeric nature. The lifetimes at 2.4-2.1 ns of the longest component of Chl *f* in Fr cells are faster than the reported lifetime at around 5.2 and 5.4 ns of isolated Chl *f* and Chl *a*, respectively, in benzene (Kobayashi et al. 2015).

We estimated the energy transfer processes in PSI and PSII of Fr cells based on the TRS and DAS analyses as diagrams in Fig. 6, in which peak positions were assigned based on DAS.

***Discussion***

*Production of Chl f in a cyanobacterium strain KC1.* A unicellular freshwater cyanobacterium strain KC1 produced Chl *f* as a minor component after growth under far-red 740-nm LED light (Akutsu et al. 2011, Ohkubo et al. 2011, Miyashita et al. 2014). The situation resembles those reported in cells of a filamentous marine cyanobacterium, *H. hongdechloris* (Chen et al. 2010), or a thermophilic filamentous cyanobacterium, *Leptolyngbya* sp. (Gan et al. 2014). The cell shapes and phylogenic locations of strain KC1, however, are significantly different from the others and rather closer to a unicellular cyanobacterium *A. marina* that produces Chl *d* (Miyashita et al. 2014). Absorption spectra of Wh and Fr cells of KC1 strain in Fig. 1 apparently resemble those in the other Chl *f*-producing organisms (Chen et al. 2010, Gan et al. 2014) although they vary somehow each other. The results in KC1 cells, as well as in *H. hongdechloris* (Chen et al. 2010), or *Leptolyngbya* sp. (Gan et al. 2014) cells, indicate that multiple species of cyanobacteria, which are distant phylogenically from each other, produce Chl *f* in adaptation to the far-red-light environments.

Chl *f* has been assumed to harvest far-red light based on its spectral feature (Chen et al. 2010, Miyashita et al. 2014) and its specific induction by far-red light (Gan et al. 2014) although it has not been fully confirmed yet. Fr cells of KC1 strain gave the high peak of Chl *f* fluorescence at 748 nm (F748) at 77 K upon the 440 nm continuous excitation (Fig. 2). It is similar to that reported in *H. hongdechloris* (Chen et al. 2010) or *Leptolyngbya* sp. (Gan et al. 2014,). Recent works analyzed fluorescence lifetime in cells (Tomo et al. 2014) and thylakoids (Akimoto et al.2 015) of *H. hongdechloris* with the 440-nm excitation laser flash and concluded that Chl *f* accepts excitation energy from Chl *a*. The present study, indicated the energy transfer from Chl *a* on PSI to multiple spectral forms of Chl *f* upon the 405-nm excitation too, and further indicated that the excitation of phycocyanin initiates the fast energy transfer to a different set of Chl *f* bands in PSII with short time constants of 0.07 and 0.33 ns even at 77 K. It is interesting whether the function of Chl *f*, revealed in this study, is similar or different in the other Chl *f*-producing cyanobacterial species.

*PSI and PSII bind different sets of Chl f.* Upon the 440-nm excitation of Fr cells, a large fluorescence peak was detected apparently at 748 nm at 77 K (F748) under continuous illumination (Fig 2). Fr cells almost lost the broad fluorescence band at 731 nm of the PSI red-Chl *a* (to less than 10%) that was the strongest fluorescence band in Wh cells. The measurement by the streak camera system in this study provided better sensitivities in the far-red region and gave fluorescence lifetimes with corrected emission spectra. The DAS analysis indicated that F748 is the longest lifetime component with a $t_c$ of 2.4 ns (Fig. 7). Fast energy transfer occurred from the excited PSI antenna Chl *a* to F690/F730/F760 and, then, to F740/F750/F760/F805 (<0.03 ns). Then,

F750/F760/F805 decayed with a $t_c$ of 0.19 ns, F740 decayed with a $t_c$ of 0.92 ns and F748 decayed with the longest $t_c$ of 2.4-ns, as summarized in Fig. 6.

Excitation of PE/PC on phycobilisome by 570-nm continuous light induced strong fluorescence with a peak at 721 nm at room temperature (Fig. 2). The 630-nm laser excitation induced F740/F760/F810 bands at 77 K (Figs. 3 and 4). F695, which can be assumed to be emitted from Chl *a* on a CP47 subunit in PSII (de Weerd et al. 2002), was also strong. DAS analysis (Fig. 5) indicated that excitation energy was rapidly transferred to Chl *f* (F720, F740/F810) bands with a $t_c$ less than 0.07-ns from PC/APC (F660) band, and then, the energy was dissipated with a 0.33-ns $t_c$ from F740/F760/F810 bands or with a 1.1-ns $t_c$ from F695/F740/F770 band. F752 exhibited the slowest decay with a $t_c$ of 2.1-ns as summarized in Fig. 6.

PSII-Chl *a* bands (F680/F695) also contributed to the 0.33- and 1.1-ns DAS showing the their decay faster than that of F752. However, the energies on F680/F695 were no more transferred to the Chl *f* bands indicating that the excitation energy is not equilibrated between F680/F695 pigments and Chl *f* molecules at the longer time scale at 77 K. It is also noted that PC/APC transferred more excitation energy to F680/F695 than to Chl *f* bands and that the Chl *a* excitation induced stronger Chl *f* fluorescence than the PC excitation did.

These results indicate the two groups of Chl *f* molecules, which are connected almost independently to PSI and PSII, as summarized in Fig. 6. A group of Chl *f* molecules emitting F730/F748/F760/F805 accepts excitation energy from Chl *a* in PSI, while the other group emitting F720/F740/F752/F760/F770/F810 accepts excitation energy from phycobilisome, presumably via Chl *a* on PSII. The longest wavelength bands, F805 and F810 may represent vibronic progressions of the shorter-wavelength Chl *f* bands because the fluorescence spectrum of Chl *f* in benzene has a major peak at 711.7 nm with a vibronic band at 750-840 nm (Fig. S2). However, the 805-810 nm band heights are high so that some portion might be emitted from the aggregated Chl *f* molecules, although it is not clear yet. Phycobilisomes do not seem to bind Chl *f* because PC transferred excitation energy to Chl *a*. F695 and the Chl *f* bands, thus, seem to be connected indirectly with each other, probably mediated by the shorter-wavelength antenna Chl *a* molecules on PSII. Chl *a* excitation gave stronger Chl *f* fluorescence bands compared to the PC excitation. It may indicate the larger amount (or tighter coupling) of Chl *f* on PSI than on PSII.

*Roles and locations of Chl f molecules*. Two different groups of Chl *f* molecules are shown to accept excitation energy in PSI and PSII. Although the probability of uphill energy transfer from Chl *f* to Chl *a* is low at 77 K, the high rates of energy transfer suggest the Chl *f* molecules to be tightly coupled to PSI and PSII and to work as antenna both in PSI and PSII at room temperature under the far-red light conditions as has been suggested (Chen et al. 2010, Gan et al. 2014). The DAS analyses of fluorescence decay in Figs.5 and 6 suggest the rapid equilibration of excitation energy

among pigments including Chl *f* inside PSI or inside PSII. The situation resembles that of the red-Chl *a* on PSI.

Multiple emission bands of Chl *f* with different energy transfer rates suggest multiple Chl *f* molecules to be located in the periphery of PSII and PSI, either bound to the pre-existing subunits or to the newly formed antenna proteins. The binding of Chl *f* to PSI well interprets the significant loss of red-Chl *a* band in Fr cells. On the other hand, Chl *f* does not seem to replace the special pair Chls in PSI and PSII because the far-red acclimation only slightly affected the absorption bands of Chl *a* as well as the PSII-specific F685/F694 bands. It is also seen that the pigment composition of Fr cells did not significantly change from that of Wh cells except for the production of Chl *f* as shown in Table 1. It is in contrast to the case in *Acaryochloris marina*, in which Chl *d* replaces almost all Chl *a*, changes full absorption and fluorescence bands, deletes both F685/F694 and the red Chl *a* bands, and has produced new special pairs P740 and P720 made of Chl *d* in PSI and PSII, respectively (Hu et al, 1998, Itoh et al. 2007, Tomo et al. 2007). The difference might come from the different affinities of pigments; Chl *d* with the high affinities even to the pre-existing Chl *a*-binding sites (Itoh et al. 2007), while Chl *f*, with the lower affinity, might occupy only the limited sites on the preexisting like the case with artificially expressed Chl *b* in cyanobacteria (Xu et al. 2001) or on newly expressed proteins. Chl *f* biosynthesis was proposed to accompany induction of new antenna proteins (Gan et al. 2014). Pigment analysis in this study has indicated 6.7 Chl *f* in 100 Chl *a* (Table 1). The amount is larger than 2.0 of Chl *a'* or 0.96 of Phe *a* suggesting bindings of multiple Chl *f* molecules to PSI and/or PSII, probably more on PSI judging from the stronger Chl *f* fluorescence upon the excitation of Chl *a*. Although the exact numbers of Chl *f* on PSI and PSII are not clear yet, the results in Table 1 suggest that KC1 Fr cells still contain PSI and PSII with the central core with mainly Chl *a* together with P700 or P680, and probably 7-13 Chl *f* altogether on PSI/PSII. The lower Phe *a* content in Fr cells suggests the decrease of PSII contents after the Far-red adaptation.

Multiple cyanobacterial species are now shown to produce Chl *f* under far-red light (Chen et al. 2010, Gan et al. 2014, Miyashita et al. 2014). The results in the present study has indicated that Chl *f* accepts excitation energy efficiently both from Chl *a* and PC/APC. The tight coupling of Chl *f* with Chl *a* in PSI, or with PC/Chl *a* in PSII suggests that excitation energy absorbed by Chl *f* is used by PSI and PSII reaction centers at room temperature. However, PSII has been known to use only the shorter-wavelength antenna pigments such as phycobilins, carotenoids, Chl *b* and Chl *c* to accumulate excitation energy to Chl *a*. Chl *f*, whose energy level is much lower than that of Chl *a*, will work rather as the energy sink to accumulate and dissipate excitation energy under visible light as seen from its fluorescence stronger than that of Chl *a* even at room temperature (Figs. 2-5 and Fig S5). This situation may not be very advantageous for the efficient collection of energy under

visible light. However, Chl *f* will be useful if only far-red light is available. It is, therefore, reasonable that Chl *f* is synthesized only under far-red light conditions, such as in dense culture, bio-mats, mud, as well as under the artificial far-red light. However, it still remains to be clarified whether all the discovered Chl *f*-producing organisms have similar sets of Chl *f* spectral forms and active P680 and P700 molecules or not. If they are similar, it may indicate the ancient origin and wide distribution of Chl *f*-production in cyanobacteria.

***Materials and Methods***

A cyanobacterium strain KC1 was collected from Lake Biwa in central Japan (Ohkubo et al. 2011, Miyashita et al. 2014). Cells were continuously grown under a white fluorescent lamp (Fl6W, Toshiba, Tokyo, Japan) at 40 μmol photons/$m^2$/s in a BG11 medium and then grown under 740 nm LED light at 30 μmol photons/$m^2$/s (STICK-FR. EYELA, Tokyo, Japan) for three weeks to accumulate Chl *f* (Akutsu et al. 2011, Miyashita et al. 2014).

Pigment contents were determined by high performance liquid chromatography (HPLC) after careful extraction of cells with acetone/methanol (7/3, v/v) mixture as described previously (Miyashita et al. 2014, Kobayashi et al. 2015). Wh and Fr cells used in the present study contained 0 and 6.7 % Chl *f*, respectively, with respect to Chl *a* as shown in Table 1.

Absorption spectra of KC1 cells suspended in a growth medium were measured with a UV-VIS spectrometer (UV-2450, SHIMADZU, Kyoto, Japan) with an integrating sphere (ISR-2200, SHIMADZU, Kyoto, Japan). Steady state florescence emission and excitation spectra were measured by a fluorescence spectrophotometer (F-2700, Hitachi, Tokyo, Japan) with a cryostat attachment (4J1-0104, Hitachi, Tokyo, Japan). It should be noted that the sensitivity of this setup falls sharply above 750 nm and has almost no sensitivity at 790 nm as described in text (compare Figs. 2 and 3) and that spectra obtained were shown without sensitivity corrections in Figs2 and S3.

Fluorescence lifetimes were measured by a streak camera system (C4780, Hamamatsu Photonics, Hamamatsu, Japan) either with a 405-nm or 630-nm diode laser (50 ps full width at a half maximum; FWHM, Hamamatsu Photonics, Hamamatsu, Japan) that is operated at 1 MHz as described previously (Yamakawa et al., 2012). Fluorescence emitted from sample cells in a liquid nitrogen cryostat (N90, Oxford Co., Oxford, UK) was focused on the entrance slit of a 50 cm monochromator to be diffracted horizontally by a grating, and then, fed into a streak camera to shift the locations of photons along the vertical axis as for their arrival times. Emitted photons, whose locations were shifted for emission wavelength horizontally and for arrival time vertically, were detected by a charge-coupled device (CCD). If the intensity of the trace is above the thermal noise level, its location on the CCD image was counted as a trace of single photon in the single photon counting mode. Obtained images were corrected as for the sensitivity of the detecting system. This

process made the emission peaks in the far-red region in Figs. 3-5 or S4, S5 to be larger and better resolved in comparison with those in Fig. 2 and S3.

Fluorescence data were further analyzed either by calculating time-resolved spectra (TRS) to see the variation of spectra at 0.1 ns intervals after the laser excitation, or by global analysis to simulate the data as the sum of decay-associated spectra (DAS), each of which gives a summed spectrum of components with the same decay-time constant ($t_c$), by home-developed programs, as reported previously (Komura et al. 2006).

***Funding***

The work was supported by JSPS KAKENHI Grant Numbers 23655196 and 26440139 to S. I.

***Disclosures***

Conflict of interest: No conflicts of interests declared.

***Acknowledgments***

Authors thank Dr. S. Ohkubo of Tsukuba University for his determination of pigment compositions. S. I. thanks Dr. Masahiro Ishiura for his kind support for the experiments.

***References***

Akimoto S, Shinoda T, Chen M, Allakhverdiev SI, Tomo, T. (2015) Energy transfer in the chlorophyll *f*-containing cyanobacterium, *Halomicronema hongdechloris*, analyzed by time-resolved fluorescence spectroscopies. Photosynth Res. 125:115-122.

Akutsu S, Fujinuma D, Furukawa H, Watanabe T, Ohnishi-Kameyama M, Ono H, Ohkubo S, Miyashita H and Kobayashi M (2011) Pigment analysis of a chlorophyll *f*-containing cyanobacterium strain KC1 isolated from Lake Biwa. Photomed. Photobiol. 33: 35–40.

Chen M, Schliep M, Willows R, Cai ZL, Neilan BA and Scheer H (2010) A red-shifted chlorophyll. Science 329: 1318–1319.

Chen M, Li Y, Birch D and Willows RD (2012) A cyanobacterium that contains chlorophyll *f*—a

red-absorbing photopigment. FEBS Lett. 586: 3249–3254.

Chen M (2014) Chlorophyll modifications and their spectral extension in oxygenic photosynthesis. Annu. Rev. Biochem. 83: 317-40.

de Weerd FL, Palacios MA, Andrizhiyevskaya EG, Dekker JP and van Grondelle R (2002) Identifying the lowest electronic states of the chlorophylls in the CP47 core antenna protein of photosystem II. Biochemistry 41: 15224–15233.

Gan F, Zhang S, Rockwell NC, Martin SS, Lagarias JC and Bryant, DA (2014) Extensive remodeling of a cyanobacterial photosynthetic apparatus in far-red light. Science 345: 1312–1317.

Gobets B, Stokkum IHM, Rögner M, Kruip J, Schlodder E, Karapetyan N, Dekker JP and van Grondelle R (2001) Time-resolved fluorescence emission measurements of photosystem I particles of various cyanobacteria, a unified compartmental model. Biophys. J. 81: 407–424.

Hirose Y, Rockwell NC, Nishiyama K, Narikawa R, Ukaji Y, Inomata K, Lagarias JC and Ikeuchi M (2013) Green/red cyanobacteriochromes regulate complementary chromatic acclimation via a photochromic photocycle. Proc. Natl. Acad. Sci. USA 110: 4974–4979.

Hu Q, Miyashita H, Iwasaki I, Kurano N, Miyachi S, Iwaki M and Itoh S (1998) A photosystem I reaction center driven by chlorophyll *d* in oxygenic photosynthesis. Proc. Natl. Acad. Sci. USA 95: 13319–13323.

Itoh S, Iwaki M and Ikegami I (2001) Modification of photosystem I reaction center by the extraction and exchange of chlorophylls and quinones. Biochim. Biophys. Acta 1507: 115–138.

Itoh S, Mino H, Itoh K, Shigenaga T, Uzumaki T and Iwaki M (2007) Function of chlorophyll *d* in reaction centers of photosystems I and II of the oxygenic photosynthesis of *Acaryochloris marina*. Biochemistry 46: 12473–12481.

Jordan P, Fromme P, Witt HT, Klukas O, Saenger W, Krauss N (2001) Three-dimensional structure of cyanobacterial photosystem I at 2.5 angstrom resolution. Nature 411: 909–917.

Kobayashi M, Sorimachi Y, Fukayama D, Komatsu H, Kanjoh T, Wada K, Kawachi M, Miyashita H, Ohnishi-Kameyama M, and Ono H (2015) Physicochemical Properties of Chlorophylls and

Bacteriochlorophylls, In "Handbook of Photosynthesis, 3rd Edition, Chapter 7", (ed. by Pessarakli M), CRC Press, in press.

Komura M, Shibata Y and Itoh S (2006) A new fluorescence band F689 in photosystem II revealed by picosecond analysis at 4–77 K, function of two terminal energy sinks F689 and F695 in PS II. Biochim. Biophys. Acta 1757: 1657–1668.

Komura K and Itoh S (2009) Fluorescence measurement by a streak camera in a single-photon-counting mode. Photosyn. Res. 101: 119–133.

Kumazaki K, Abiko K, Ikegami I, Iwaki M, Itoh S (2002) Energy equilibration and primary charge separation in chlorophyll *d*-based photosystem I reaction center isolated from *Acaryochloris marina*. FEBS Lett. 530: 153-157.

Lewin RA (2002) Prochlorophyta – a matter of class distinctions. Photosynthesis Research 73: 59–61.

Li Y, Scales N, Willows RD, Blankenship RE and Chen M (2012) Extinction coefficient for red-shifted chlorophylls, chlorophyll *d* and chlorophyll *f*. Biochim Biophys Acta 1817: 1292–1298

Li Y, Cai ZL and Chen M (2013) Spectroscopic properties of chlorophyll *f*. J. Phys. Chem. B. 117: 11309–11317.

Mielke SP, Kiang NY, Blankenship RE, Gunner MR and Mauzerall D (2011) Efficiency of photosynthesis in a Chl *d*-utilizing cyanobacterium is comparable to or higher than that in Chl *a*-utilizing oxygenic species. Biochim. Biophys. Acta. 1807: 1231–1236.

Miller SR, Augustine S, Olson TL, Blankenship RE, Selker J and Wood A (2005) Discovery of a free-living chlorophyll *d*-producing cyanobacterium with a hybrid proteobacterial cyanobacterial small-subunit rRNA gene. Proc. Natl. Acad. Sci. USA 102: 850–855.

Miyashita H, Ikemoto H, Kurano N, Adachi K, Chihara M and Miyachi S (1996) Chlorophyll *d* as a major pigment. Nature 383: 402.

Miyashita H, Adachi K, Miyachi S, Chihara M, Ikemoto H and Kurano N (1997) Pigment

composition of a novel oxygenic photosynthetic prokaryote containing chlorophyll *d* as the major chlorophyll. Plant Cell Physiol. 38: 274–281.

Miyashita H, Ohkubo S, Komatsu H, Sorimachi Y, Hukayama D, Fujinuma D, Akutsu S and Kobayashi M (2014) Discovery of chlorophyll *d* in *Acaryochloris marina* and chlorophyll *f* in a unicellular cyanobacterium, strain KC1, isolated from Lake Biwa. J. Phys. Chem. Biophys. 4: 10004.

Murakami A, Kim S-J and Fujita Y (1997) Changes in photosystem stoichiometry in response to environmental conditions for cell growth observed with the cyanophyte *Synechocystis* PCC 6714. Plant Cell Physiol. 38: 392–397.

Murakami A, Miyashita H, Iseki M, Adachi K and Mimuro M (2004) Chlorophyll *d* in an epiphytic cyanobacterium of red algae. Science 303: 1633.

Niedzwiedzki DM, Liu H, Chen M and Blankenship RE (2014) Excited state properties of chlorophyll. Photosyn. Res. 121:25-34.

Ohkubo S, Usui H and Miyashita H (2011) Unique chromatic adaptation of a unicellular cyanobacterium newly isolated from Lake Biwa. Japan. J. Phycol. (Sorui) 59, 52(A22) (in Japanese).

Schliep M, Crossett B, Willows RD and Chen M (2010) 18O-labelling of chlorophyll *d* in *Acaryochloris marina* reveals that chlorophyll *a* and molecular oxygen are precursors. J. Biol. Chem. 285: 28450–28456

Sugiura K and Itoh S (2012) Single-cell confocal spectrometry of a filamentous cyanobacterium *Nostoc* at room and cryogenic temperature. Diversity and differentiation of pigment systems in 311 cells. Plant Cell Physiol. 53: 1492-1506.

Swingley WD, Chen M, Cheung PC, Conrad AL, Dejesa LC, Hao J, Honchak BM, Karbach LE, Kurdoglu A, Lahiri S, Mastrian SD, Miyashita H, Page L, Ramakrishna P, Satoh S, Sattley WM, Shimada Y, Taylor HL, Tomo T, Tsuchiya T, Wang ZT, Raymond J, Mimuro M, Blankenship RE and Touchman JW (2008) Niche adaptation and genome expansion in the chlorophyll *d*-producing cyanobacterium *Acaryochloris marina*. Proc. Natl. Acad. Sci. USA 105: 2005–2010.

Tomo T, Shinoda T, Chen M, Suleyman IA and Akimoto S (2014) Energy transfer processes in chlorophyll *f*-containing cyanobacteria using time-resolved fluorescence spectroscopy on intact cells. Biochim. Biophys. Acta 1837: 1484–1489.

Tomo T, Okubo T, Akimoto S, Yokono M, Miyashita H, Tsuchiya T, Noguchi T and Mimuro M (2007) Identification of the special pair of photosystem II in a chlorophyll *d*-dominated cyanobacterium. Proc. Natl. Acad. Sci. USA 104: 7283–7288.

Umena, Y, Kawakami, K , Shen, JR, Kamiya, N (2011) Crystal structure of oxygen-evolving photosystem II at a resolution of 1.9 angstrom. Nature 473: 55–65.

Willows RD, Li Y, Scheer H and Chen M (2013) Structure of chlorophyll *f*. Org. Lett. 15: 1588–1590.

Xu H, Vavilin D and Vermaas W (2001) Chlorophyll *b* can serve as the major pigment in functional photosystem II complexes of cyanobacteria. Proc. Natl. Acad. Sci. USA 98: 14168–14173.

Yamakawa H, Fukushima Y, Itoh S, Heber U (2012) Three different mechanisms of energy dissipation of a desiccation-tolerant moss serve one common purpose: to protect reaction centres against photo-oxidation. J. Exp. Bot. 63, 3765-75.

Table 1. Pigment contents in KC1 cells grown under white (Wh) and 740 nm (Fr) light.

| | Chl *f* | Chl *a'* | Pheo *a* |
|---|---|---|---|
| Fr cells (% of Chl *a*) | 6.7 | 2.0 | 0.96 |
| Wh cells (% of Chl *a*) | 0 | 2.1 | 0.64 |

Pigment contents are expressed with respect to 100 Chl *a* molecules. Contents in Fr and Wh cells are mean values of 21-24 and 6 analyses, respectively, with error ranges of around 14 %. See Materials and Methods, and Kobayashi et al (2015) for detailed procedures.

***Figure Legends***

Figure 1. Absorption spectra of KC1 cells grown under white (Wh) and far-red (Fr) light. Blue and red lines indicate spectra of Wh and Fr cells, respectively. The two spectra were measured with an integrating sphere, and normalized at the 680-nm Chl *a* peak. Inset shows a microscopic image of KC1-Fr cells.

Figure 2. Steady state fluorescence emission spectra of Wh and Fr cells at room temperature and at 77 K. a and c, fluorescence emission spectra of Wh cells at room temperature and 77 K, respectively. b and d, spectra of Fr cells at room temperature and 77 K, respectively. Spectra were obtained with either 440-nm (red line) or 570-nm (blue line) excitation light. Curves in lower cases indicate $2^{nd}$ derivative spectra calculated from the spectra in a-d. Vertical bars indicate apparent peak positions determined on the basis of the $2^{nd}$ derivative spectra. Note that the intensities in the figure are not corrected as for the lower detector sensitivities above 700 nm.

Figure 3. Time-wavelength two-dimensional images of fluorescence detected in Fr cells. Top, at 300 K excitated by 405- (a) and 630-nm (b) excitation lasers. Middle, at 77 K with 405- (c) and 630-nm (d) excitations. (e) and (f), integrated fluorescence emission spectra at 77 K with 405- (e) and 630-nm (f) excitations. A thin line in (e) also shows the integrated 630-nm excited spectrum same as that in (f) as for comparison. These spectra in e and f were calculated by integrating the intensities along whole 5-ns time range in images (c) and (d), respectively. These spectra should be equivalent to those in Fig. 2c after the sensitivity-correction of the latter. The laser profiles were measured separately in a different wavelength ranges, and are not shown. All the data were corrected as for detector sensitivities.

Figure 4. Time-resolved fluorescence emission spectra (TRS) in Fr cells at 77 K after excitations at 405 (a) and 630 nm (b). Each TRS was calculated by summing up fluorescence intensities within a 0.1 ns time range with a central delay time at -0.12, 0, 0.12, 0.37, 0.86, 1.7 or 4.2 ns with respect to the peak time of excitation laser pulse. The spectra were calculated from the image data at 77 K in Fig. 3.

Figure 5. Decay associated spectra (DAS) calculated for the fluorescence in Fr cells. Upper images, at room temperature with excitations at 405 (a) and 630 nm (b). Lower images at 77 K with excitations at 405 (c) and 630 nm (d). DAS were calculated from the images in Fig. 3 with respect to the indicated time constants that were obtained by a global analysis program as described in

Figure 6. Schematic diagrams for the energy transfer process in PSII in Fr cells at 77 K. Arrows represent energy transfer from Chl *a* to indicated Chl *f* fluorescence bands in PSI, and from phycocyanin to indicated Chl *a* and Chl *f* fluorescence bands. The diagrams are drawn based on the analysis in Figs 4 and 5. See text for details.

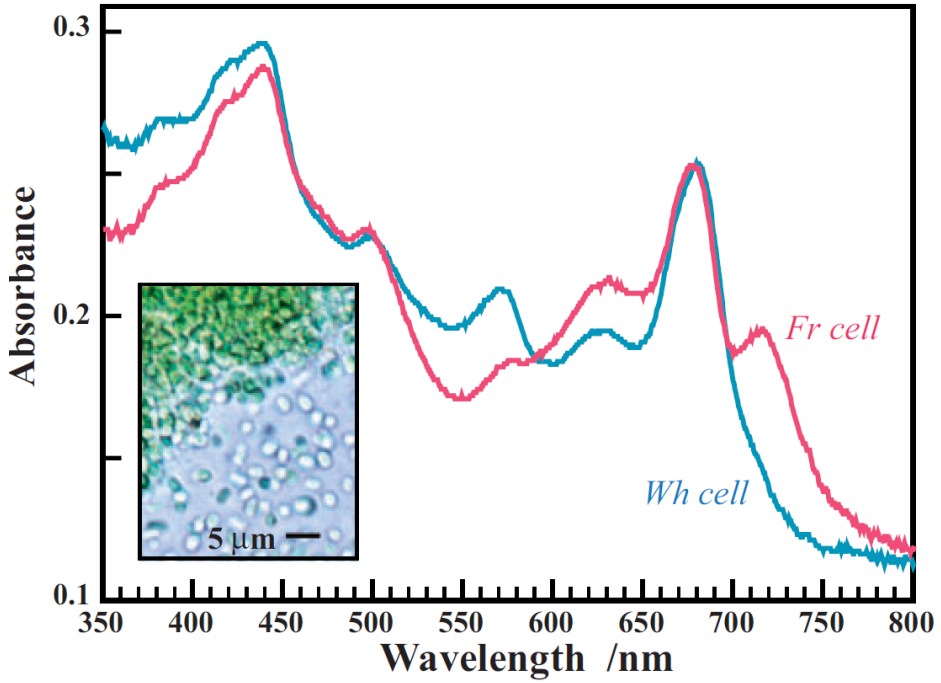
0.3
0.2
0.1
Absorbance
350
400
450
500
550
600
650
700
750
800
Wavelength /nm
Fr cell
Wh cell
5 μm

Figure **1**

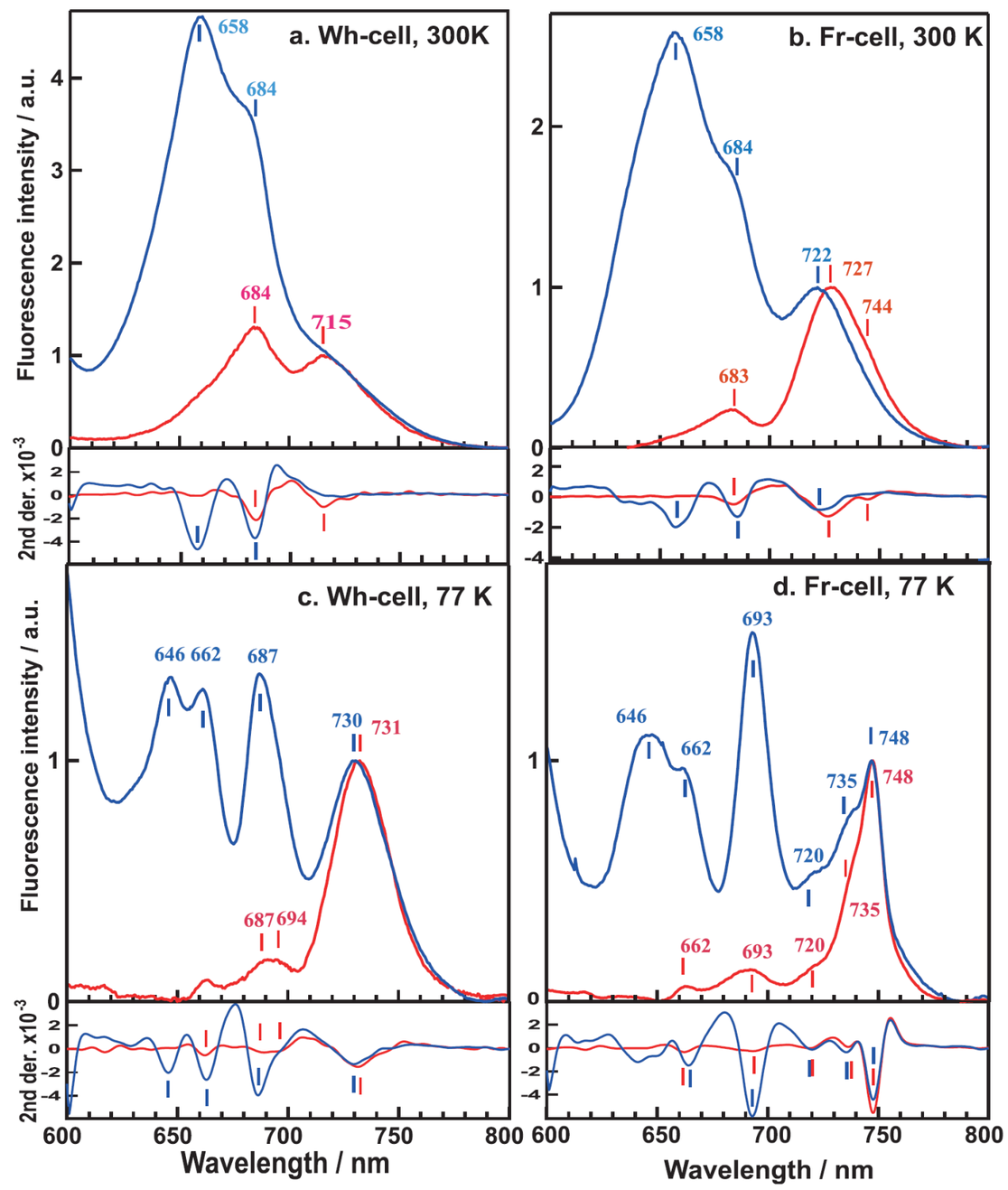
a. Wh-cell, 300K
658
684
684
715
b. Fr-cell, 300 K
658
684
722
727
744
683
c. Wh-cell, 77 K
646 662
687
730
731
687 694
d. Fr-cell, 77 K
693
646
662
748
735
748
720
735
662
693
720
Fluorescence intensity / a.u.
2nd der. x10-3
Wavelength / nm

Figure **2**

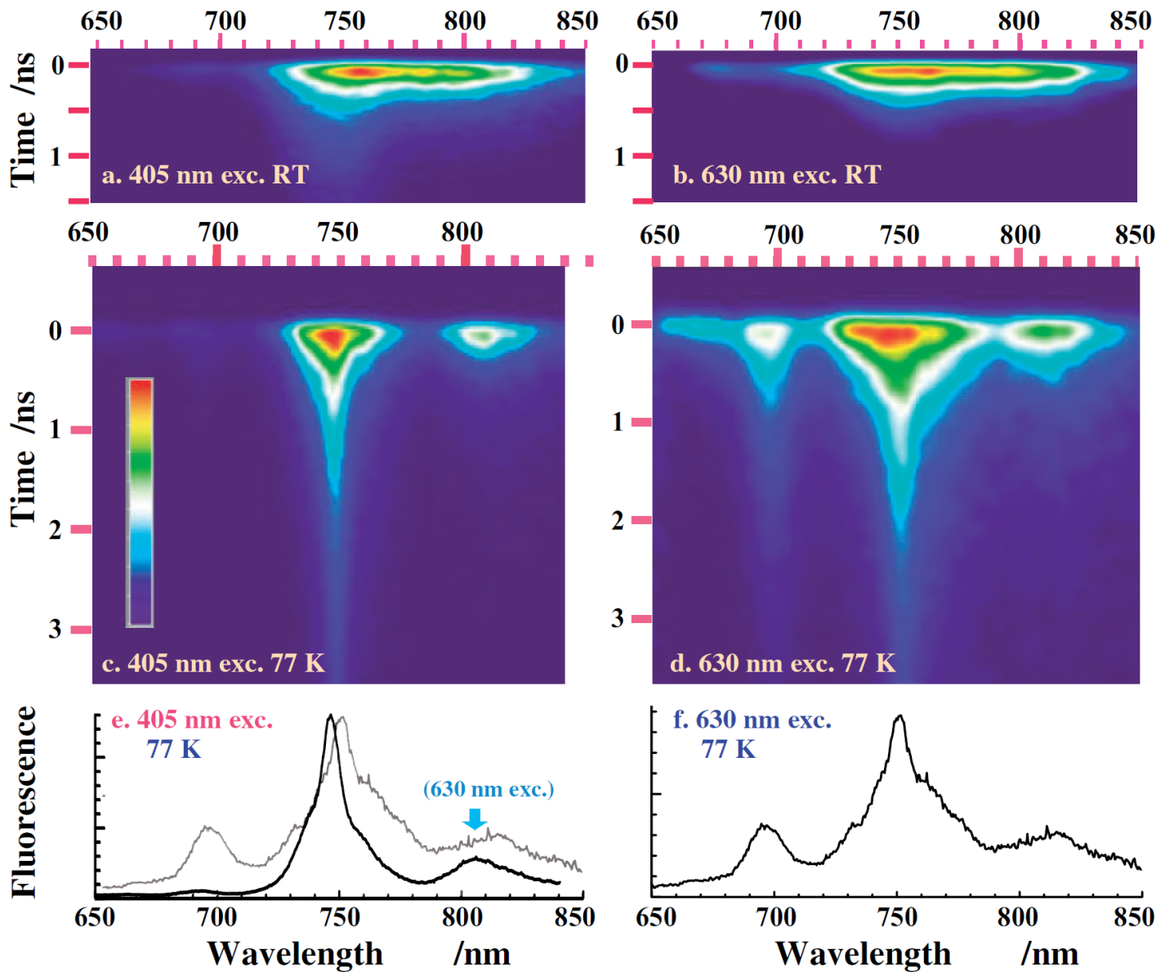
650
700
750
800
850
Time /ns
0
1
a. 405 nm exc. RT
b. 630 nm exc. RT
2
3
c. 405 nm exc. 77 K
d. 630 nm exc. 77 K
Fluorescence
e. 405 nm exc.
77 K
(630 nm exc.)
f. 630 nm exc.
77 K
Wavelength /nm

Figure **3**

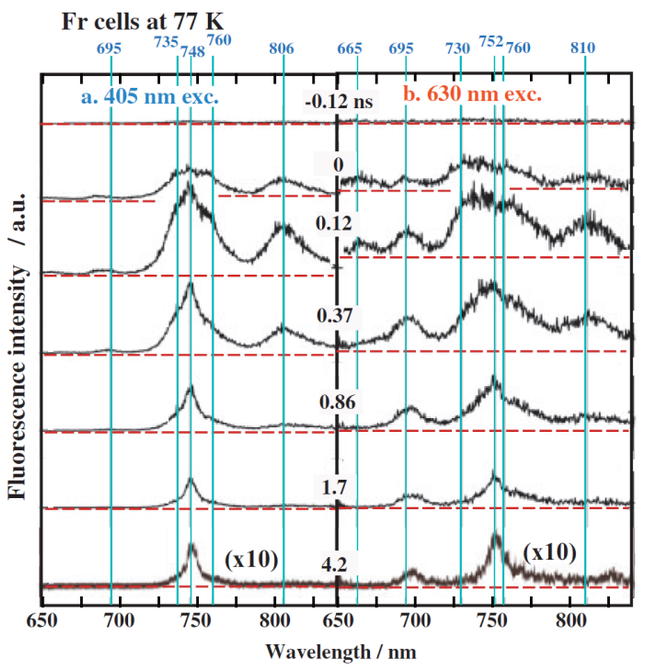
Fr cells at 77 K
695
735
748
760
806
665
695
730
752
760
810
a. 405 nm exc.
b. 630 nm exc.
-0.12 ns
0
0.12
0.37
0.86
1.7
4.2
(x10)
(x10)
Fluorescence intensity / a.u.
650
700
750
800
650
700
750
800
Wavelength / nm

Figure **4**

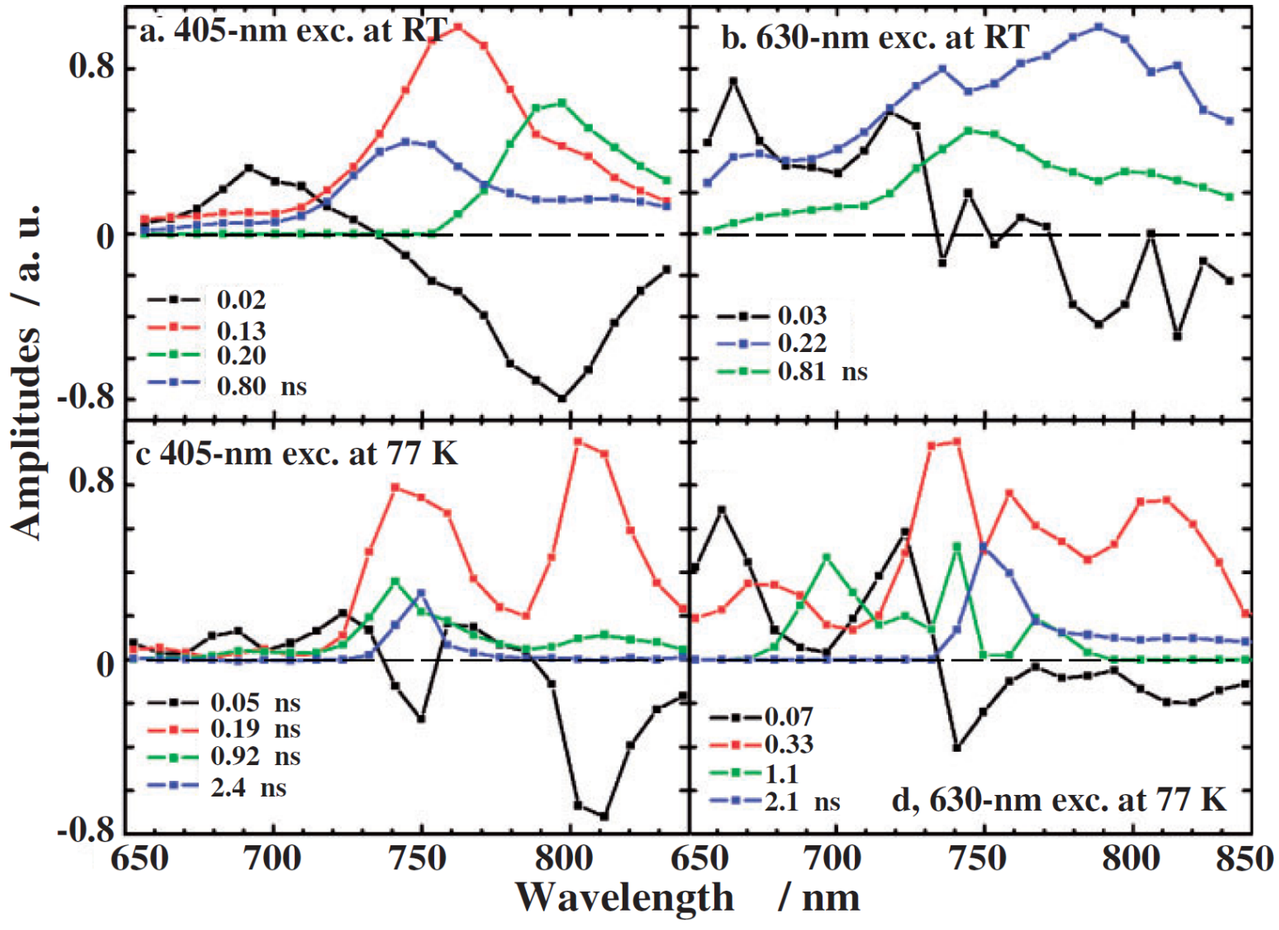
a. 405-nm exc. at RT
b. 630-nm exc. at RT
c 405-nm exc. at 77 K
d, 630-nm exc. at 77 K
0.02
0.13
0.20
0.80 ns
0.03
0.22
0.81 ns
0.05 ns
0.19 ns
0.92 ns
2.4 ns
0.07
0.33
1.1
2.1 ns
0.8
0
-0.8
650
700
750
800
850
Amplitudes / a. u.
Wavelength / nm

Figure **5**

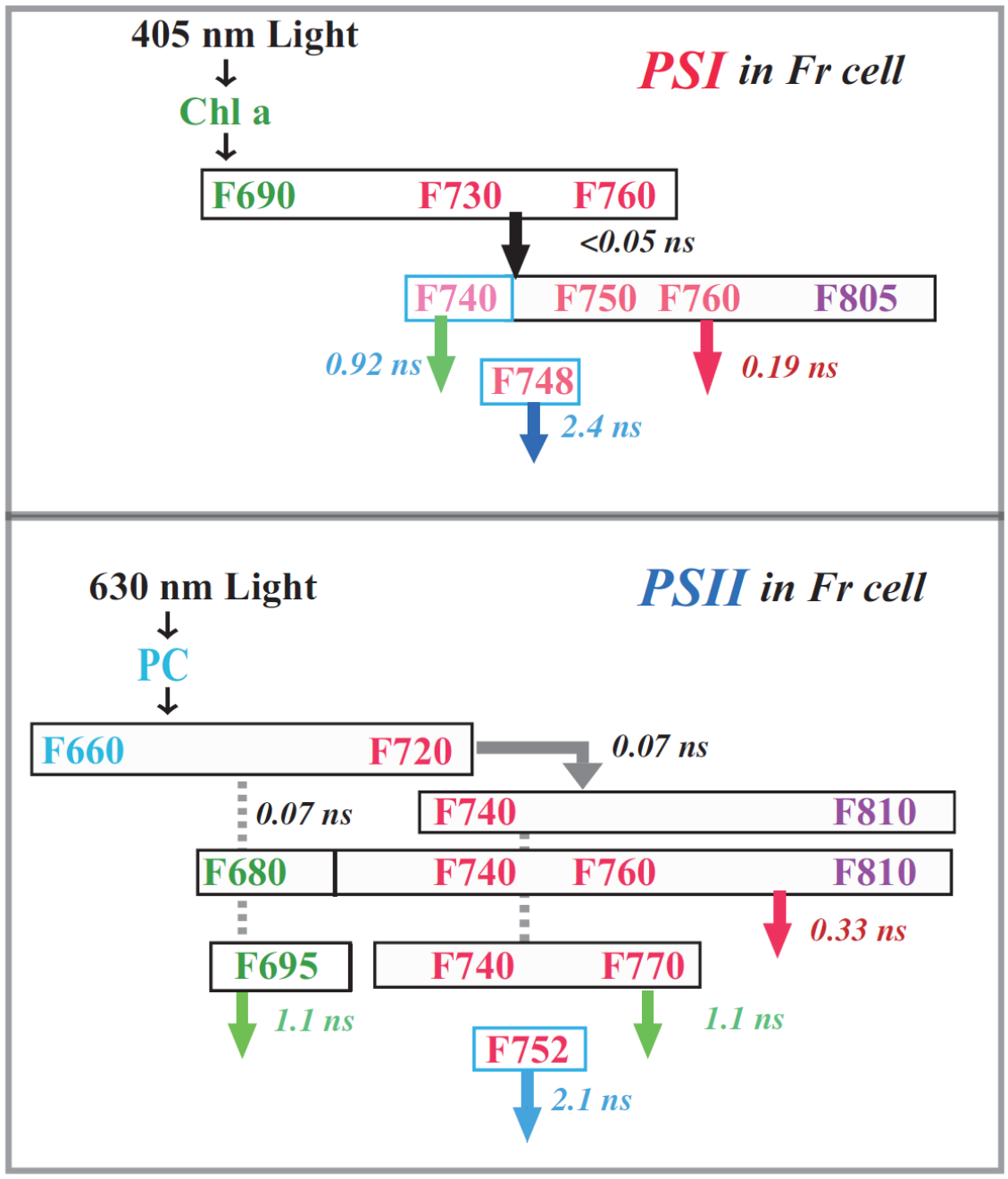
405 nm Light
Chl a
PSI in Fr cell
F690
F730
F760
<0.05 ns
F740
F750
F760
F805
0.92 ns
F748
0.19 ns
2.4 ns
630 nm Light
PC
PSII in Fr cell
F660
F720
0.07 ns
0.07 ns
F740
F810
F680
F740
F760
F810
0.33 ns
F695
F740
F770
1.1 ns
1.1 ns
F752
2.1 ns

Figure 6

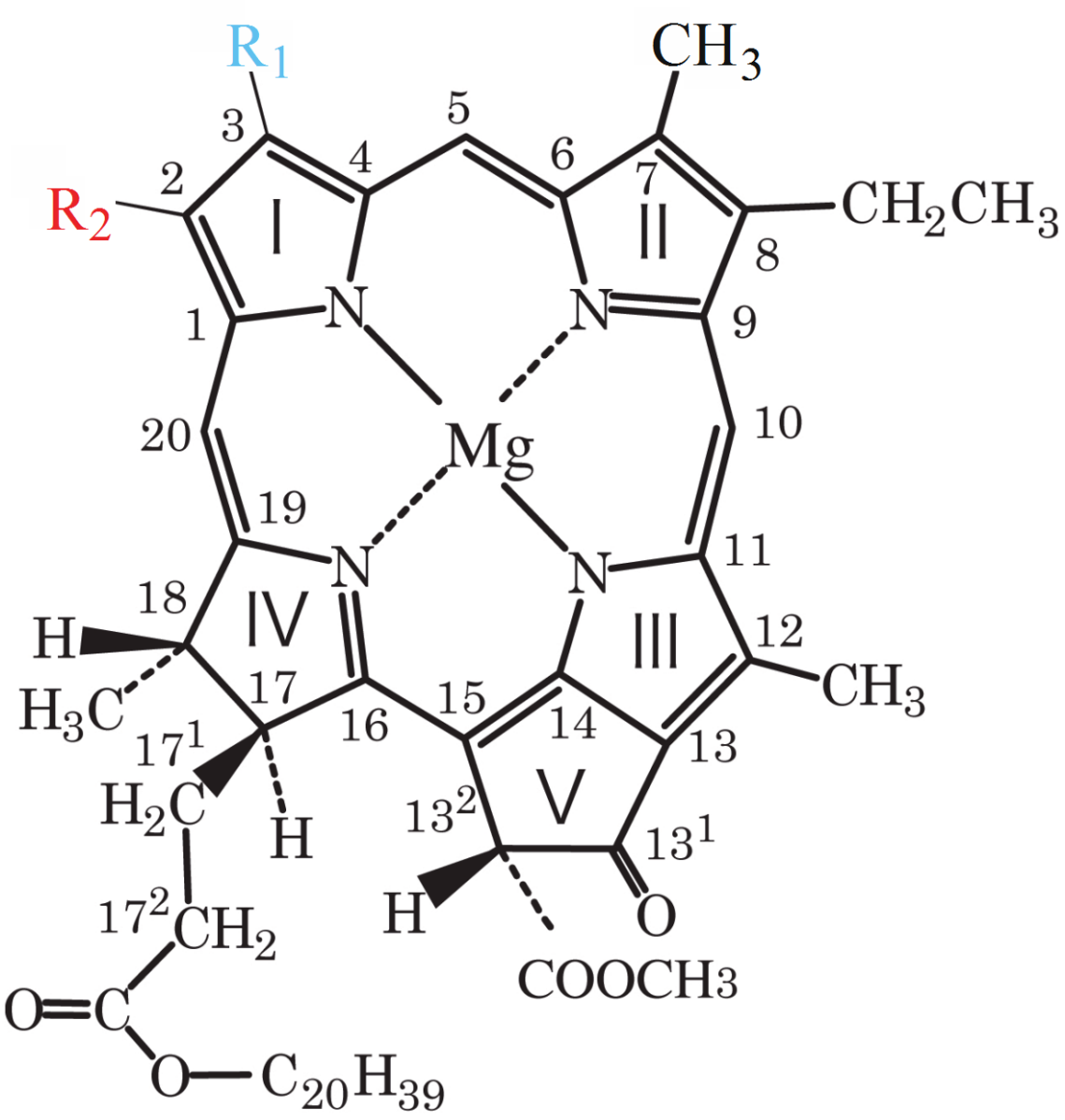


| | $R_1$ | $R_2$ |
|---|---|---|
| Chl *a* | $CH_3$ | $CH{=}CH_2$ |
| Chl ***f*** | $CH_3$ | CHO |
| Chl ***d*** | CHO | $CH{=}CH_2$ |

Figure S1. Chemical structures of chlorophyll *a*, *d* and *f*. Modifications of chlorophyll *a* structure to add -CHO group as R1 or R2 give Chl *d* or Chl *f*, respectively.

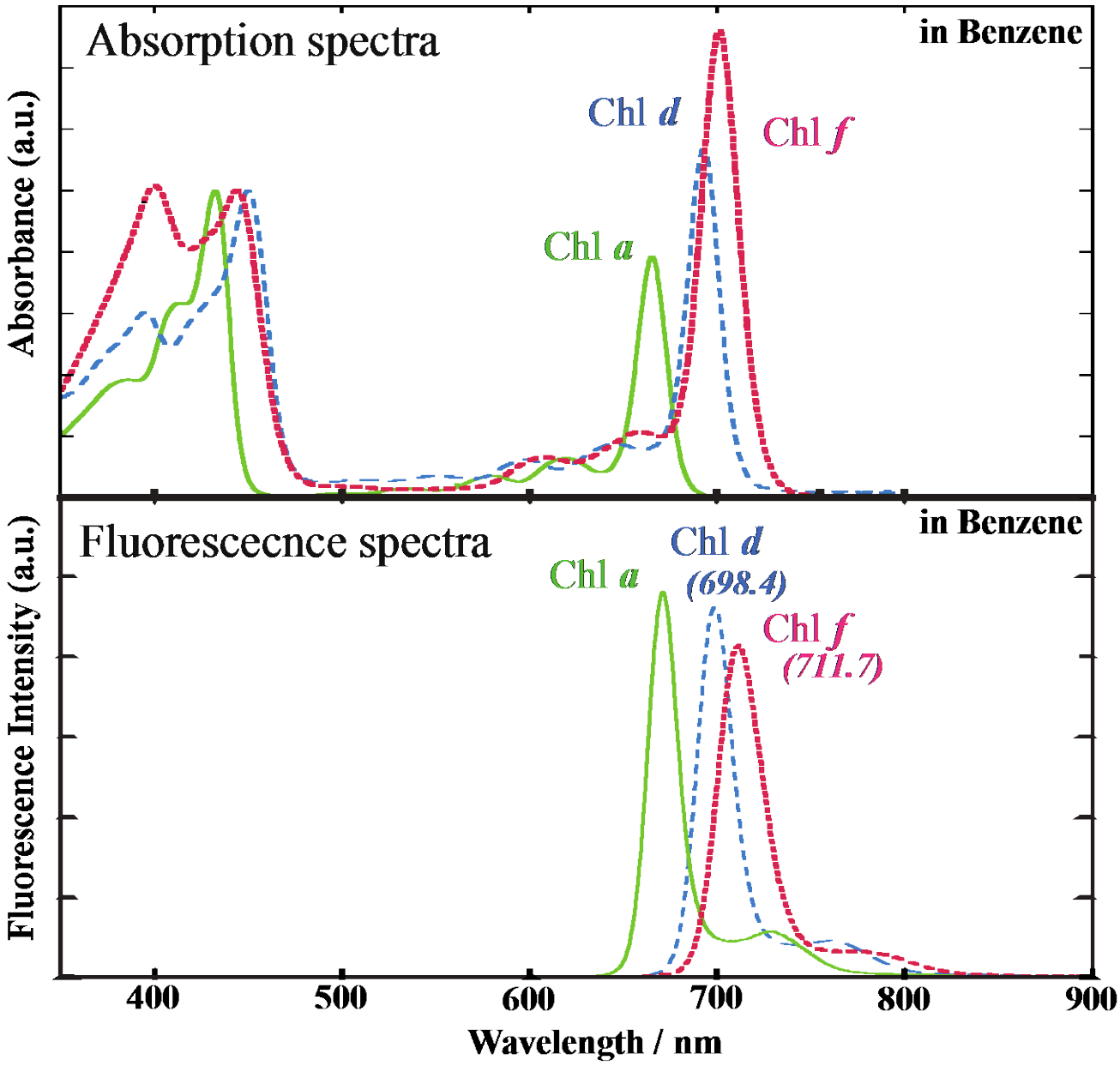


Figure S2. Absorption and fluorescence emission spectra of purified Chl *a*, *d*, *f* dissolved in benzene measured at room temperature. Absorption spectra are normalized at Soret peaks. Peak wavelengths of fluorescence emission are shown in brackets. The spectra were obtained as described in Kobayashi et al. (2015).

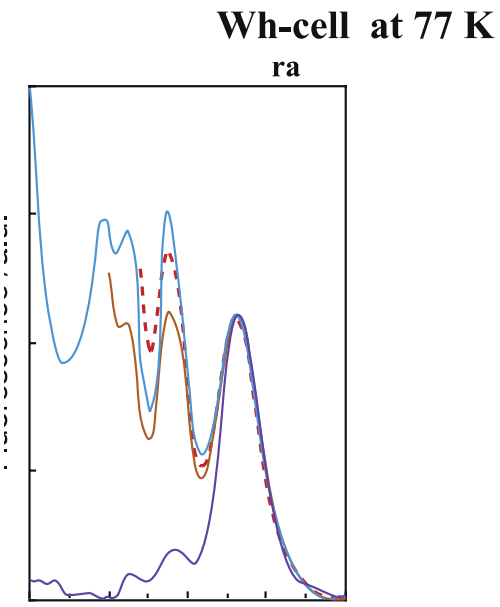


Figure S3. Fluorescence emission and excitation spectra, respectively, of Wh cells (a, b) and Fr cells (c, d) at 77 K measured under continuous illumination with a conventional apparatus. Spectra were not corrected as for detector sensitivities.

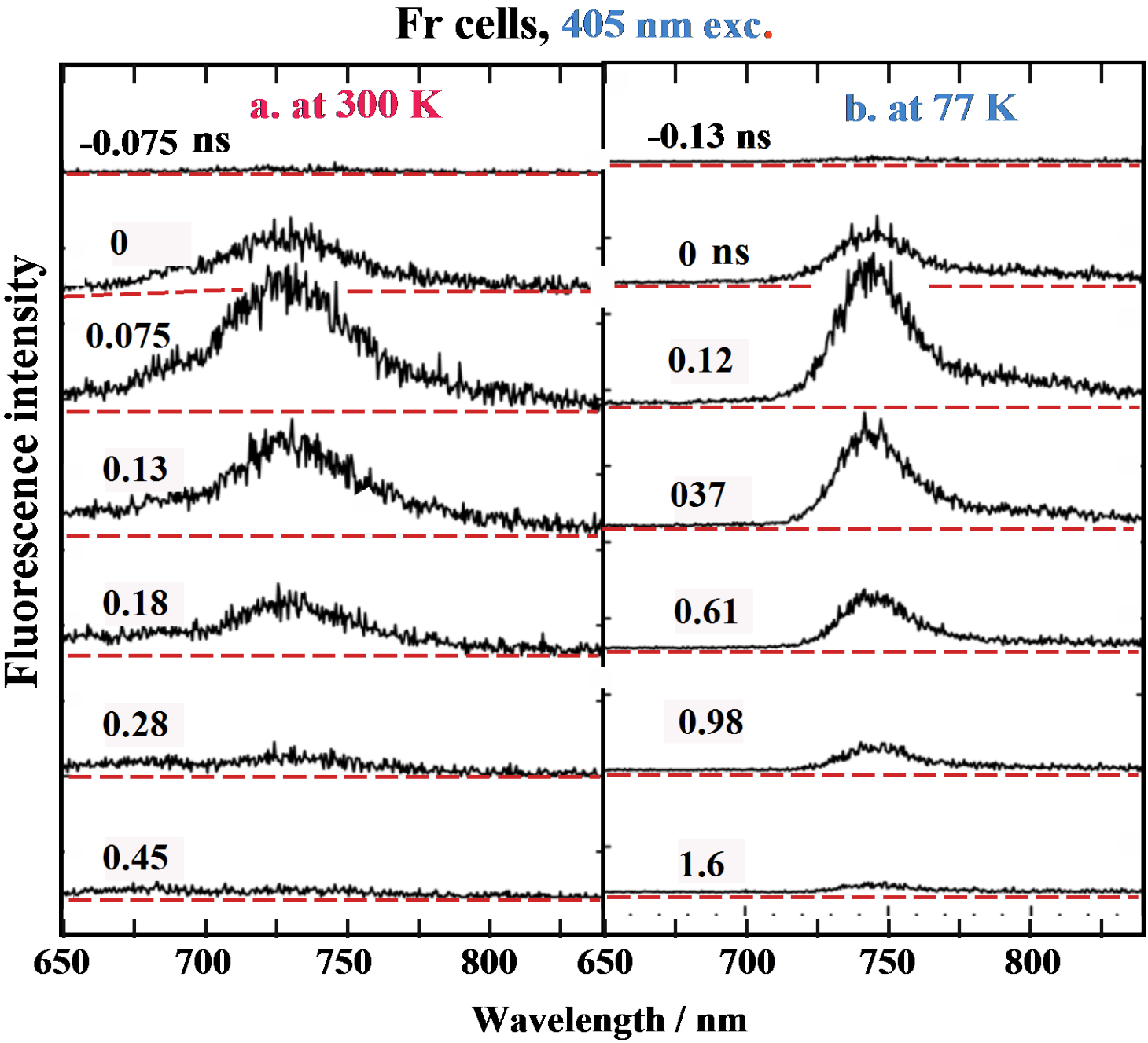


Figure S4. Time-resolved fluorescence emission spectrum (TRS) in Wh cells at 300 K (a) and at 77 K (b) after excitation at 405 nm. TRS was calculated by summing up intensities within a 0.1 ns time range with a central delay time as indicated in the figure with respect to the peak time of excitation laser pulse. Fluorescence spectra comprise of PSII Chl *a* and PSI red-Chl *a* bands at around 680 nm and at around 735 (300K) – 745 nm (77K), respectively.

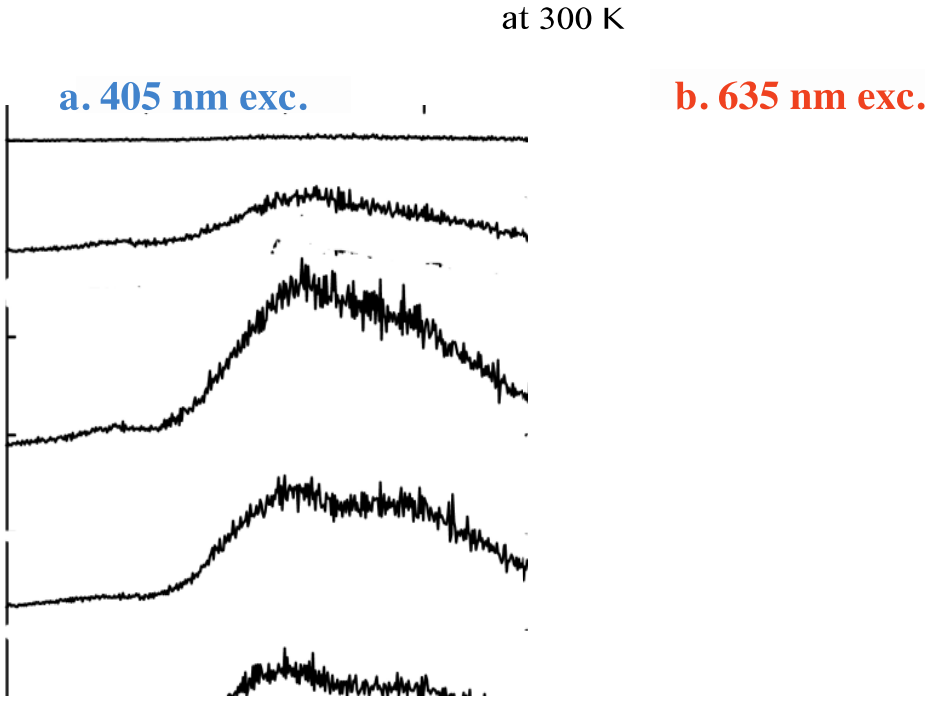


Figure S5. Time-resolved fluorescence emission spectrum (TRS) in Fr cells at 300 K after excitations at 405 (a) and 630 nm (b). TRS was calculated by summing up intensities within a 0.1 ns time range with a central delay time as indicated in the figure with respect to the peak time of excitation laser pulse. Chl *a* in PSII gives fluorescence at around 680-690 nm, while different spectral forms of Chl *f* give bands at 720-850 nm.